Astron. Astrophys. 360, 761–776 (2000)

ASTRONOMY AND ASTROPHYSICS

Multi-component structure of solar and stellar transition regions

H. Peter

Kiepenheuer-Institut für Sonnenphysik, Schöneckstrasse 6, 79104 Freiburg, Germany (peter@kis.uni-freiburg.de)

Received 28 April 2000 / Accepted 16 May 2000

Abstract. Emission lines from the solar transition region between the chromosphere and the corona often show a two Gaussian component profile with a core and a broad second component contributing up to 25% to the total intensity. For the first time a systematic study of the broadening *and* Doppler shift of the second weaker components is performed using SUMER on SOHO to explore the spatial structures of the second components.

It is found that the two component structure is basically restricted to the bright chromospheric network. The narrow core component shows the familiar transition region redshifts, with hardly any blueshifts in the network. The broad second components are blueshifted compared to the core, but are still predominantly redshifted. However, quite large areas in the network (up to $20'' \times 20''$) show concentrations of blueshifts in the second component. In the inter-network the line profile has a single Gaussian shape and shows small red- and also some blueshifts.

It is suggested that the two components in the network correspond with two spatially unresolved physical regimes in quiet Sun network: small scale loops and larger scale coronal loop structures anchored in the network. The footpoint regions of the latter are of a funnel-type and form a "canopy" above inter-network regions of the chromosphere. Shocks propagating upward from the non-magnetic chromosphere interact with this canopy, which leads to the transition region inter-network emission. A further analysis, especially of emission lines originating from higher temperatures, is required to confirm this scenario.

The distribution and correlations of the line intensities, shifts and widths show that these physical regimes are heated by different mechanisms. This sheds new light on the interpretation of stellar observations in terms of coronal heating. A comparison to existing studies of stellar transition regions shows the need for more thorough theoretical investigations on the formation of stellar transition region lines.

Key words: Sun: transition region – Sun: corona – stars: coronae – line: profiles

1. Introduction

The transition region from the chromosphere to the corona of the Sun and similar stars is the ideal region to study the energy transport from the photosphere to the corona to heat the latter. Spatially, temporally *and* especially spectrally resolved data of emission lines originating from the transition region provide the best tool to study the underlying physical processes. These lines are most common in the EUV region, i.e. from about 500 Å to 2000 Å.

In the past, several instruments were used to investigate these lines, e.g. the HRTS spectrograph on rocket flights and on-board Spacelab, or the OSO instruments. The most recent high-resolution instrument is the SUMER spectrograph (Solar Ultraviolet Measurements of Emitted Radiation, Wilhelm et al. 1995) on-board SOHO.

The profiles of (optically thin) lines can provide information on waves and/or mass motions transporting energy into the corona, because these processes lead to observable signatures such as non-thermal line broadening and line shifts, even in data that are unresolved spatially. This can be measured by a spectrograph, like SUMER, which is an important advantage compared to imaging filter-graph instruments.

Previous spectral investigations concentrated mostly on the properties of the line core, i.e. a single (Gaussian) component was assumed and an analysis of the moments of the line or a single Gaussian fit was performed. However, about two decades ago it was found that emission lines from the middle transition region, like C IV (1548, 1550 Å), Si IV(1394, 1403 Å) or C III (1909 Å), show a significant deviation from a single Gaussian shape. Kjeldseth Moe & Nicolas (1977) were the first to show this for solar spectra obtained through a $2'' \times 60''$ aperture instrument on Skylab and interpreted the enhanced emission in the wings as due to a second Gaussian component. The excess in the wings is too strong to be understood by damping, i.e. by a Voigt-profile. The second components are much weaker, contributing about 5–25% to the total line intensity, and much broader (by a factor 2) than the line core. It took more than a decade before these results were re-examined – Dere & Mason (1993) analysed rocket flight HRTS data, with roughly $1''$ spatial resolution. In their extensive study they summarised results on the non-thermal broadening of the line cores and the broad second Gaussian components and interpreted these in terms of wave energy transport and coronal heating.

This effect is not specific for our own star, the Sun. Detailed work on the transition region line profiles and extended wings was done using Hubble Space Telescope (HST) data by Wood et al. (1997) and references cited therein. They applied double Gaussian fits to line profiles from a number of stars

spanning activity levels comparable to the Sun to high activity (e.g. AU Mic, AB Dor). They found the excess in the wings to be increasing with activity, which means that the second minor Gaussian component is broader in comparison to the core component for more active stars. They interpreted this in terms of microflaring, explosive events or prominences.

The most important difference between the stellar and the solar work is that the stellar profiles do not have any spatial resolution, while for solar profiles one is able to resolve structures below the scale of the granulation and well below the supergranular scale of the chromospheric network. The importance of the solar work for the stellar interpretation is to provide information where these second components originate from (at least for solar-type stars). On the other hand when searching for physical explanations of the solar observations, one should favor processes that agree with the activity run of the second component properties of a larger number of stars.

The present paper presents the analysis of a data set from the SUMER instrument that is large enough to provide significant statistical results on the line shifts *and* the widths not only of the line core but especially of the second components. The existing data sets from previous instruments were simply too small to achieve this aim. This was due to the limited amount of time e.g. during a rocket flight, and/or lower quality (photographic) detectors.

2. Data analysis

2.1. Observations

The data presented in this paper were acquired during a SUMER raster scan on September 22, 1996, i.e. during solar minimum. The data cover a $540'' \times 300''$ region of quiet Sun centered at solar (x,y) $\sim(-200'', 430'')$, i.e. at $\sim 25^\circ$ heliocentric angle to the north-east. For the scan 181 horizontal steps were performed with a step size of $3''$. As the $1''$ wide slit was used one has to keep in mind that the Sun was significantly under-sampled.[1] The spectra covered 1531 Å – 1552 Å (1st order) and were observed with the KBr part of detector A. This wavelength range includes among others the C IV (1548 Å) line from the transition region, which is analysed in the current paper. To obtain a better signal-to-noise ratio the data are spatially binned along the slit (3 pixels) leading to an actual resolution element of $1'' \times 3''$. Together with the long exposure time of 150 s for a single spectrum this is sufficient to allow for a reliable double Gaussian fit.

This data set was chosen for a meaningful comparison between results on the "traditional" line core analysis and the core component of the double Gaussian fit presented in this paper. These data have already been used by Dammasch et al. (1999) to analyse the core of C IV in terms of a moment analysis and by Hassler et al. (1999) to study the coronal source of the solar wind by fitting single Gaussian profiles to the Ne VIII line.

[1] The "Schmierschritt" (smear step) procedure, where the slit is moved during the exposure time to avoid under-sampling, was not applied here.

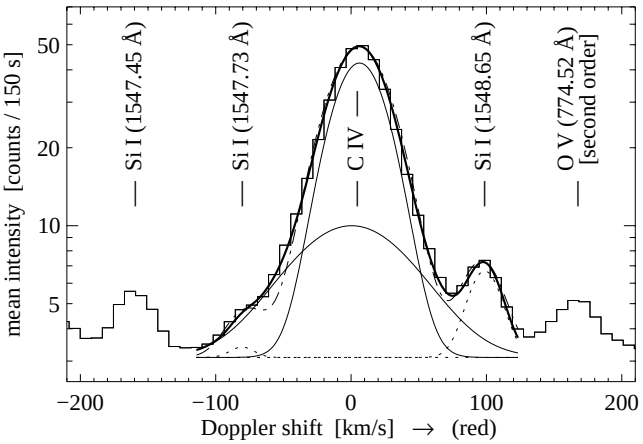

Fig. 1. Quiet Sun as a star. Mean spectrum of C IV (1548 Å) of the whole field of view. The observed spectrum is shown in histogram mode. Over-plotted is a four component Gaussian fit (thick solid) accounting not only for the core and the second component of C IV (thin solid), but also fitting the two clearly resolved weak blends of Si I at 1547.73 Å and 1548.65 Å (dotted). The dotted-dashed line shows the fit if only a single Gaussian is used to approximate the C IV profile. Please note the logarithmic scale, i.e. the two blends contribute less than ∼4% to the total intensity in the spectral region shown here, while the second component contributes ∼20%. The fit parameters are listed in Table 1.

2.2. Data reduction and Gaussian fits

Standard correction procedures (flat field and geometric distortion) as well as additional corrections for temporal drifts and left-overs from the geometric correction have been applied (see e.g. Peter 1999 for technical details). A wavelength calibration was applied by using chromospheric lines in the observed spectral window.

The main step in the data reduction was to extract parameters for a reliable double Gaussian fit with a constant continuum. In this study the Genetic Algorithm based optimisation method implemented by Charbonneau (1995) was used. This algorithm already proved extremely stable in the reduction of other SUMER spectra (e.g. Peter 1999). The main advantage of such a *global* optimisation algorithm is its superb performance even with low signal-to-noise data. As not only the main core component of the spectral line, but also a second, much weaker and broader component has to be fitted, the robustness of the algorithm to produce meaningful fits in the presence of noise is of vital importance.

As can be seen from the mean spectrum of the whole field of view shown in Fig. 1 there are two weak blends in the outer wings of the C IV line. These are Si I lines at 1547.73 Å and 1548.65 Å. In principle these lines have to be fitted simultaneously with the core and the second component of C IV to obtain the best result. However, for the individual spectra it is sufficient to fit only the two C IV components for the following two reasons: First both blends lie far out in the wings (note that all spectra shown in this paper are on a logarithmic scale, which emphasises the wings). They are at a distance of ∼80 and $\sim 100\,\mathrm{km\,s^{-1}}$ in the blue and red wing respectively and

Table 1. Quiet Sun as a star. Parameters for the double Gaussian fit of C IV (1548 Å) for the mean spectrum shown in Fig. 1. Doppler shift $v_{\rm D}$ (positive is red), line width $\triangle v_{1/e}$ and non-thermal broadening ξ for the core and the second component. R is the ratio of the total intensity of the second to the core component. For comparison also the parameters for a single Gaussian C IV fit are shown. By comparing the $\chi^2_{\rm r}$ it is apparent that the double Gaussian fit is superior.

	$v_{\rm D}$	$\triangle v_{1/e}$	ξ		
	[km s^{-1}]			R	$\chi^2_{\rm r}$
core component	6.2	15	10	} 25%	0.95
second component	0.5	36	35		
single Gaussian fit	5.9	18	14	–	3.5

contribute less than ∼4% compared to the C IV core. Second – and this is the main reason not to consider these blends when fitting the C IV profiles – the individual profiles are much narrower than the mean profile. This is because in the mean profile some Doppler shifts are not resolved that are resolved in the individual spectra, which leads to an additional broadening. The broadening due to not-resolved motions obviously increases for poorer resolution. This leads to the conclusion that in the individual spectra the two "blends" are well separated from C IV, which is confirmed by the sample spectra shown in Fig. 4. In addition the fitting algorithm allows to build in constraints, which were used here, amongst others, to keep the second component from fitting one of the blends.

In the present paper the line widths will be given in Doppler widths $\triangle v_{1/e}$ of the respective Gaussians $\exp(-v^2/\triangle {v_{1/e}}^2)$. This relates to the full width at half maximum as $\mathrm{FWHM} = 2\sqrt{\ln 2}\,\triangle v_{1/e}$. All the line widths listed in tables or in the text are corrected for instrumental broadening by using the standard SUMER procedure con_width_funct_2. For a better comparison the fitted Gaussians shown with the observed profiles are plotted including the instrumental broadening.

2.3. Single vs. double Gaussian fits

For all spectra a double and also a single Gaussian fit was performed (respectively with a constant continuum). The reason for this is twofold: on one hand this allows a comparison between the two fits (through the reduced $\chi^2_{\rm r}$ statistic) which enables one to distinguish between regions where a second component is present and where one component is sufficient to describe the data. On the other hand this can serve as a double check, because the results for the single Gaussian fit should not differ too much from the core component of the double Gaussian fit. Finally the single Gaussian fits can be compared to previous studies of the same data set (Dammasch et al. 1999).

In this study the following criteria are used to decide whether a double Gaussian fit is required and reliable. (1) $\chi^2_{\rm r}$ of the double Gaussian fit has to be 0.9 or less of the single Gaussian fit, i.e. the detection of the second component must significantly improve the value of $\chi^2_{\rm r}$. (2) $\chi^2_{\rm r}$ for the fit has to be below 1.5, i.e. the fit has to be reliable. In the remainder of the paper, those regions where both requirements are fulfilled will be called "*two component regions*". If only requirement (2) is fulfilled, but the values of $\chi^2_{\rm r}$ for the double and single Gaussian fit are comparable, the region will be called "*single component region*". If neither criterion is fulfilled, the respective spectra, called "bad", will not be considered.

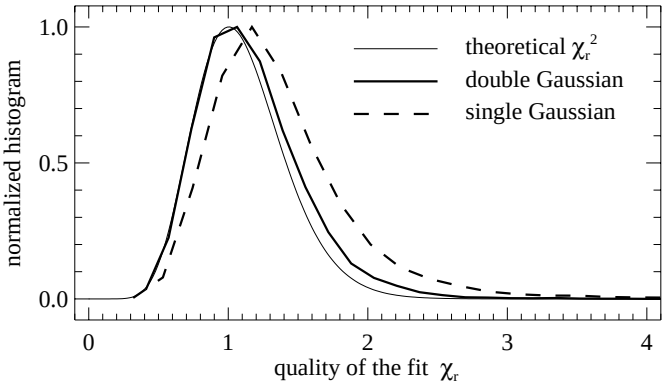

Fig. 2. Distribution of $\chi^2_{\rm r}$ for all single and double Gaussian fits with the latter being close to the theoretical optimal distribution and superior to the former one.

In Fig. 2 the (normalised) distributions of the reduced $\chi^2_{\rm r}$ of the whole data set for the single and the double Gaussian fits are shown. The thin line shows the theoretical distribution (Poisson statistics), depending only on the number of data points and the number of parameters for the fit (e.g. Bevington & Robinson 1992). It is obvious from this figure that in general the double Gaussian fits are superior to the single Gaussian fits and their distribution of χ^2 is close to the theoretical optimal curve. The $\chi^2_{\rm r}$ have been calculated assuming Poisson statistics for the error σ of the count rate, i.e. σ is given by the square root of the counts.

This clearly shows the need for a double Gaussian fit in a substantial fraction of the observed data and demonstrates the high quality of the fits. In Sect. 3.1 it will be shown further that the double Gaussian fits are required mostly in the bright network elements, while the single Gaussian fits seem to be sufficient in most parts of the inter-network.

3. Observational results

3.1. Spatial structure: the network

As the data studied in this paper cover a rather large area of $540'' \times 300''$, the spatial structure of the Doppler shifts and line widths of both the narrow core and the broad second component can be investigated with statistical significance.

The results of the double Gaussian fits are displayed in Fig. 3. The left panel shows the parameters for the core, the right panel for the weaker second component. In the images of the second component all those data points are masked in green where the second component was not detectable. Areas where the double Gaussian fit is not reliable are masked in black (see Sect. 2.3).

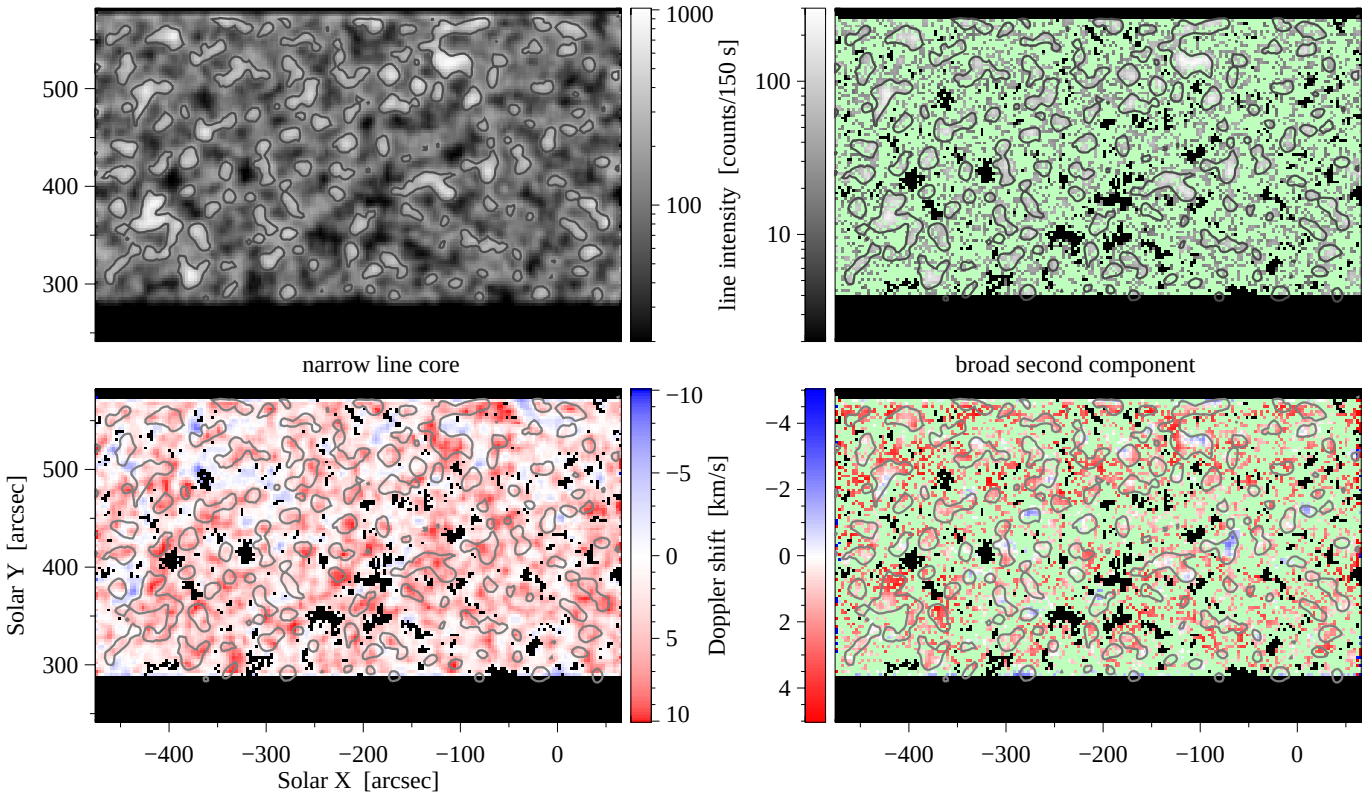

Fig. 3. Spatial image of the line intensity and the line shift of the line core (left) and the second component (right). In the images showing the second component all points, where no second component could be detected, are blended out in green. The black areas mark regions where the signal was too low to perform a reliable fit at all. The contours enclose the bright "network". Please note that the images are plotted using square pixels, but the data are under-sampled by a factor of 3 in the solar X direction.

The contours in all plots show the network structure. These are defined by smoothing the intensity image of the core component and then defining the value for the contour line "by eye" to separate the bright network. Even though this procedure is subjective the resulting contour lines and the coverage do not depend critically on the choice of the contour level because of the smoothing. The fraction of area covered by bright network is about 13%, which agrees well to Dere et al. (1984). If also the darker network structures would be considered, the coverage of the network would be about 50%, which is in agreement with Gallagher et al. (1998).

It is clearly evident from Fig. 3 that a second component is detected almost only in the bright network elements. This could simply be a signal-to-noise effect, as in the darker inter-network the signal might be too low to detect a second component, even if it would be there. But when studying the individual spectra it becomes evident that this is not the case and the second components are indeed restricted to the network.

In Fig. 4 three example spectra are shown: In the bright network (4a) the non-single-Gaussian structure is clearly evident and a double Gaussian fit is excellent. In the "not too dark" inter-network (4b) a double Gaussian fit results in one Gaussian fitting the line and another trying "to be a continuum", i.e. becoming as wide as possible. Practically this double Gaussian fit is identical to a single Gaussian fit with a continuum (in addition to the "real" continuum fitted to the spectrum). In this case a double Gaussian fit is not better than a single Gaussian fit and the spectrum does not show any convincing indication of a second component.[2] A second component of comparable relative strength (25%) as seen in the network (4a) would be detectable also for count rates as low as in the inter-network (4b). Only in the darkest inter-network regions (4c) the low signal-to-noise ratio would prevent the detection of a 20–25% broad second component. In that example less than one count every 10 s was detected at line center!

In Fig. 3 it appears that the emission from the second component shows smaller patches than from the line core. This is not a real effect though, but caused by the sharp selection criteria for spectra consisting of a single or a double Gaussian profile (Sect. 2.3). In the left panel of Fig. 3 the line intensity and shift for the line cores of the double Gaussian fits in the bright network and the respective parameters for the single Gaussians in the inter-network are shown together (for the single Gaussians the whole line profile is the core). For this reason the images on the left panels look more smooth and the right panels for the second components of only the network are more patchy.

The conclusion from the above discussion is that in the inter-network a simple single component Gaussian fit is sufficient

[2] A second component with nearly the same shift and width as the core could be present, but this is not detectable, in principle.

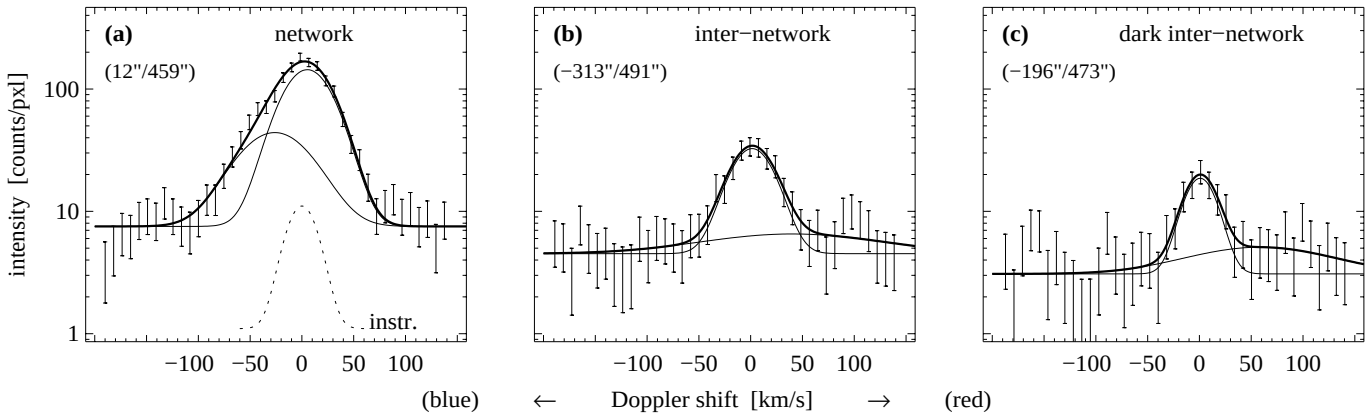

Fig. 4a–c. Sample spectra in C IV in the network and inter-network. The observed spectra are shown by the bars representing the errors. Over-plotted are the respective double Gaussian fits (thick) together with the two components (thin). Note that in contrast to the mean spectrum (Fig. 1) the two lines at −80 and 100 km s^{-1} are normally separated from the individual C IV profile. In the network spectrum **(a)** the two components are clearly visible, in the inter-network spectra the second component is either not present **(b)** or not detectable because of the low signal-to-noise ratio **(c)**. The numbers with the plots give the solar (X,Y) coordinates, where the spectra were observed (cf. Fig. 3). The dotted line shows a Gaussian with a width of the instrumental broadening.

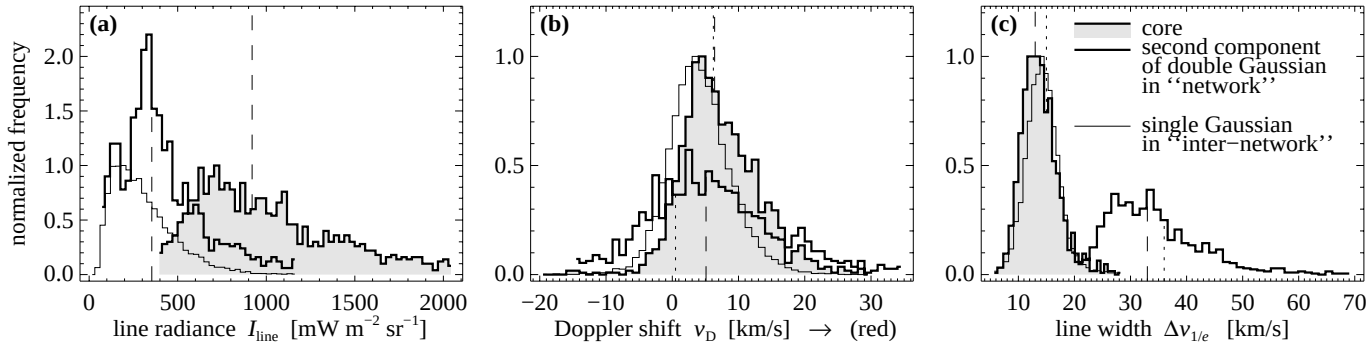

Fig. 5a–c. Histograms of line intensities, Doppler shifts and line widths. These are shown for the cores (thick, with gray shaded background) and second components (thick) in regions where double Gaussian fits are required and reliable, i.e. mainly in the network. The histograms for the single Gaussians in regions where a single Gaussian fit is sufficient, i.e. mainly inter-network, are shown as thin lines. The vertical dashed lines from above and below show the median values for the core and second components of the double Gaussian fits, respectively. The vertical dotted lines indicate the parameters for the double Gaussian fit of the *mean* C IV spectrum (Fig. 1, Table 1). See Sect. 3.2 for a discussion.

to describe the data adequately. But almost everywhere in the bright network elements a two Gaussian fit is needed. With the definitions in Sect. 2.3 the network corresponds (nearly) to the "two component region" and the inter-network to the "single component region". "Bad data" are found almost only in the darkest inter-network areas. This result shows that the network is made up of at least two major physical regimes (Sect. 4.1).

3.2. Line intensities, widths and shifts

The core component of the double Gaussian fits (left panels of Fig. 3) shows nearly the same spatial structure as is well known from a single Gaussian fit. The line is broader and shifted towards the red all over the bright network, while the shifts are small in the inter-network.

The second component, however, does not show only red-shifts in the network, but a more even distribution with more regions showing no shifts or slight blueshifts (right panels of Fig. 3). But judging by eye from images is very subjective, e.g. because of the choice of the colour table. Therefore the distribution of line intensities, widths and shifts will now be studied quantitatively.

For this purpose the respective fit parameter is analysed in the following way. The histograms for the core and second components in the "two component regions" (i.e. mainly network, see Sect. 2.3) are plotted along with the histogram of the respective parameters of the single Gaussian fit in the "single component region" (i.e. mainly inter-network). The histograms are shown in Fig. 5, the median values are listed in Table 2. Even though over-plotting the single Gaussian parameter confuses the plots somewhat, it allows for a comparison between the inter-network and the network as seen in the line core. The histograms are normalised, i.e. the maximum value of the histograms for the single Gaussians and the cores of the double Gaussian fits are set to 1. The histograms for the second com-

Table 2. Median values as derived from the distributions shown in Fig. 5. Listed are the intensities of C IV (1548 Å) integrated over the line, $I_{\rm line}$, the resulting solar surface flux, $F_\odot$, emission measures, EM_V and EM_h, the Doppler shift $v_{\rm D}$ (positive is red), line width corrected for instrumental broadening, $\triangle v_{1/e}$, and the non-thermal broadening, ξ. These values are given for the core and second components where a double Gaussian fit is required (mainly network) as well as for the single Gaussian fits that are sufficient in most places of the inter-network. For the intensity derived values also weighted means for network and inter-network are listed (13% network, 87% inter-network emission). For a comparison with stars the disk center values for $F_\odot$ have to be multiplied by ∼2.1 to get the disk average values (limb brightening). See Sect. 3.2.

median values		$I_{\rm line,\,C\,IV}$	$F_{\odot,\,\rm C\,IV}$	$\log_{10}\mathrm{EM}_V$	$\log_{10}\mathrm{EM}_h$	$v_{\rm D}$	$\triangle v_{1/e}$	ξ
		[W m^{-2} sr^{-1}]	[W m^{-2}]	[cm^{-3}]	[cm^{-5}]	[km s^{-1}]		
network (N):	core component	0.92	2.9	42.5	26.3	6.3	13	
	second component	0.35	1.2	42.1	25.9	5.1	33	31
inter-network (IN):	single Gaussian fit	0.27	0.9	42.0	25.7	3.1	15	9
weighted mean (0.13×N + 0.87×IN)		0.40	1.3	42.2	25.9			

ponents of the double Gaussian fits are shown on the same scale as the core components.

3.2.1. Intensity distribution

To be independent of the non-thermal broadening of the line profiles the total (or line) intensities (radiances) of the Gaussian components are compared, i.e. the respective contribution integrated over wavelength, $I_{\rm line} = \int I_\lambda \,\mathrm{d}\lambda$. A SUMER standard data reduction software converts the observed counts into a radiance, $I_{\rm line}$, which is measured in W m^{-2} sr^{-1}. Please note that 1 mW m^{-2} = 1 erg cm^{-2} s^{-1}. For an extended (i.e. spatially resolved) object like the Sun the radiance (or the intensity) is independent of the distance R of the observer: while the photon flux is decreasing as $1/R^2$ the observed region within the solid angle 1 sr is increasing as R^2 with increasing distance. The histograms of the resulting radiances are plotted in Fig. 5a, the median values are listed in Table 2.

As expected the core components in the network are brighter by a factor of about 3 compared to the inter-network single Gaussians. *All* the intensity histograms are not symmetric but have extended wings towards higher intensities. On average the second component in the network contributes about 25% to the total intensity of the line profile (i.e. second:core ∼ 1:3).

It should be noted that the weak second component in the network is still brighter than the emission from the inter-network by about 30%.

For a better comparison to stellar work also the solar surface fluxes $F_\odot$ of the respective components are listed in Table 2 (or more exactly the average radiant flux projected back to the solar surface). The radiance, $I_{\rm line}$, translates into a (mean) solar surface flux by simply multiplying with π, $F_\odot\,[\mathrm{W\,m^{-2}}] = \pi\, I_{\rm line}\,[\mathrm{W\,m^{-2}\,sr^{-1}}]$.[3] The data presented in the present paper are based on observations in low latitudes (∼25°, see Sect. 2.1).

Because of the center-to-limb brightening the surface fluxes $F_\odot$ as listed in Table 2 are lower than the value averaged over the solar disk, $\overline{F_\odot}$. Wilhelm et al. (1998) find a disk averaged quiet Sun irradiance of 59.2 μW m^{-2} at 1 AU corresponding to a solar surface flux of $\overline{F}_{\odot,\rm C\,IV} = 2.7\,\mathrm{W\,m^{-2}}$. Their value of 28.2 μW m^{-2} at 1 AU for ∼25° off center (415 mW m^{-2} sr^{-1}) yields a factor of 2.1 between mid latitude observations as presented in the present study and disk averaged value. The mean value for $F_{\odot,\rm C\,IV}$ (∼25°) listed in Table 2 agrees well with the Wilhelm et al. (1998) study.

For comparison with former studies of e.g. explosive events also the emission measures by volume and height, $\mathrm{EM}_V = \int n_{\rm e}^2\,\mathrm{d}V$ and $\mathrm{EM}_h = \int n_{\rm e}^2\,\mathrm{d}h$, are listed in Table 2 (see Appendix A).

3.2.2. Doppler shift distribution

The histograms for the Doppler shifts are displayed in Fig. 5b. They are basically Gaussian and show a small differential shift between the core and the second component in the network.

The core component shows the well known redshifts. The distribution is nearly Gaussian with a wide spread of the Doppler shifts; a Gaussian fitted to the histogram would have a width of about 8 km s^{-1}.

In contrast the distribution of the second components is not only broader (spread about 11 km s^{-1}), but also less weighted towards the red. While only 7% of the core components show a blueshift, more than 25% of the second components are blueshifted. The median values of the Doppler shift distributions of the core and the second components are 6 km s^{-1} and 5 km s^{-1}, respectively.

Inspection of Fig. 3 also reveals another major difference between the line shifts of the line core and the second component. While practically all of the network is redshifted, there are quite some regions that definitely show blueshifts in the second component where the core is redshifted, e.g. at solar (X,Y) $\sim (-80, 420)$. These regions can be as large as 20″×20″, i.e. much larger than the spatial resolution of the instrument.

In previous studies it was not possible to study the spatial distribution of the shifts of the second components in a statistically meaningful way.

[3] This is because the (mean) flux F at a distance R, given by a simple symmetric expansion, $F = (R_\odot/R)^2 F_\odot$, equals the radiance $I_{\rm line}$ multiplied by the area of the solar disk $\mathcal{A}_\odot\,[\mathrm{sr}] = \pi(R_\odot/R)^2$. See also e.g. Wilhelm et al. (1998).

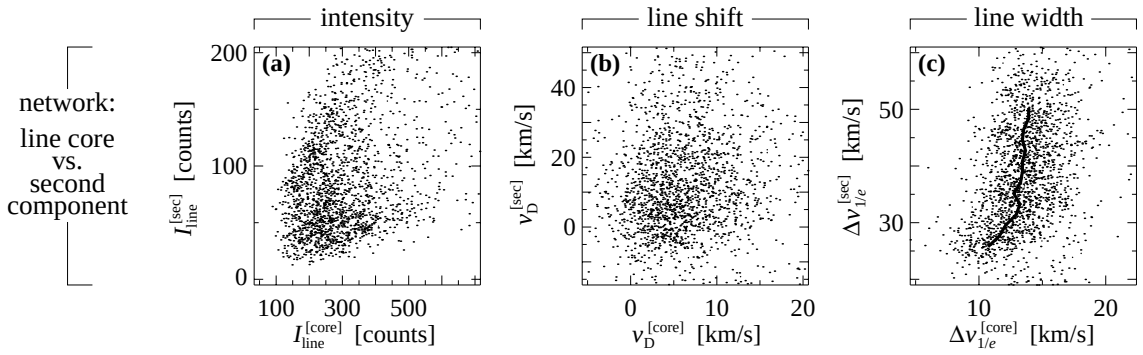

Fig. 6a–c. Correlation of line intensities $I_{\rm line}$, Doppler shifts $v_{\rm D}$ and line widths $\triangle v_{1/e}$ between the core and second components ($^{\rm [core]}$, $^{\rm [sec]}$) for the double Gaussian fits in the network. Positive values of $v_{\rm D}$ correspond to redshifts. The solid line shows the median variation.

3.2.3. Line width distribution

The histograms of the line width of the Gaussian components are plotted in Fig. 5c. The distributions for the core components in the network and the single Gaussians in the inter-network are more or less of Gaussian shape. The width of the histograms is about the thermal speed for C IV at its formation temperature at 10^5 K ($\sim$8.2 km s^{-1}).

As in the previous study of Dere & Mason (1993) the second component is found to be much broader. The median values of the distributions are found to be 13 km s^{-1} and 33 km s^{-1} for the core and the second component. Because of the much better statistics of the present data also the shape of the second component histogram can be analysed and is found to be clearly non-Gaussian with an excess to higher line widths.

It is useful to compare the line widths to the (adiabatic) sound speed $v_{\rm s}\sim$48 km s^{-1} at the formation of C IV, i.e. at 10^5 K. Comparing this sound speed with the histogram in Fig. 5c shows that the bulk of the plasma has line widths of the second components well below the sound speed. Only a minor fraction, the very tail of the distribution, exceeds the sound speed.

3.3. Correlations of the double Gaussian fits

To investigate the connections between line intensities, Doppler shifts and widths one can study scatter plots of the fit parameters. As with the histograms the narrow core and the broad second component in the network are compared to the single Gaussian inter-network profiles. Because the number of these spectra is large (couple of 1000), the statistical results on the correlations are reasonable and significant.

Scatter plots of line intensities, shifts and widths between the core and the second components in the network are shown in Fig. 6. The intensities as well as the Doppler shifts of the two components do not show any correlation, the scatter plot is just a "cloud". In contrast the widths of the second components are increasing with the widths of the core of the profile as indicated by the heavy line which connects the median values.

In Fig. 7a–f the correlations of width and shift to intensity are shown for the cores (left) and second components (middle) of the network spectra and the single Gaussian profiles from the inter-network (right), respectively. The correlation of shift to width is shown as well in panels g–i, even though this information is redundant.

For the core components there is a weak correlation between line width and intensity (7a), while there is no significant trend between line shift and intensity (7d). At first sight this is contrary to the results of Peter (1999) who found a strong correlation between shift and intensity from full Sun rasters. But one has to keep in mind that the scatter plot shown here represents only the network. This shows that the shift-intensity relation as found by Peter (1999) indicates just the cell-network-structure, as discussed in that paper, but that in the network itself no shift-intensity relation is found for the line core emission.

In contrast to the core emission the second components show strong correlations between intensity, shift and width (middle panels in Fig. 7). What is most striking is that the correlation of width and intensity for the second components (7b) is opposite to the core components (7a). Also the shift-intensity relation for the second components (7e) shows that the redshifts are stronger for lower intensities, which is opposite to the cell-network structure of the line cores (Peter 1999).

The emission from the inter-network, which is sufficiently characterised by a single Gaussian profile, shows yet another set of correlations (right panels in Fig. 7). The three parameters of the Gaussian fits are (weakly) correlated to each other, but in a different way from those of the second components from the network.

The implications of these results of the scatter plots will be discussed in terms of the transition region structure in Sect. 4.

3.4. Quiet Sun as a star: mean spectrum

To compare the Sun with other stars it is useful to look at the mean spectrum of the whole field of view. As the mean spectrum shown here represents a large enough area on the Sun (about 10% of the solar disk) it might be considered as a quiet-Sun-as-a-star spectrum. Because the region covered in the present data is near disk center the mean spectrum misses the effects of the limb brightening of C IV. A "real" Sun-as-a-star spectrum would therefore be weighted more with the emission from near the limb. As there is a strong center-to-limb variation in the Doppler shift, but not in the line width (see e.g. Peter 1999) the

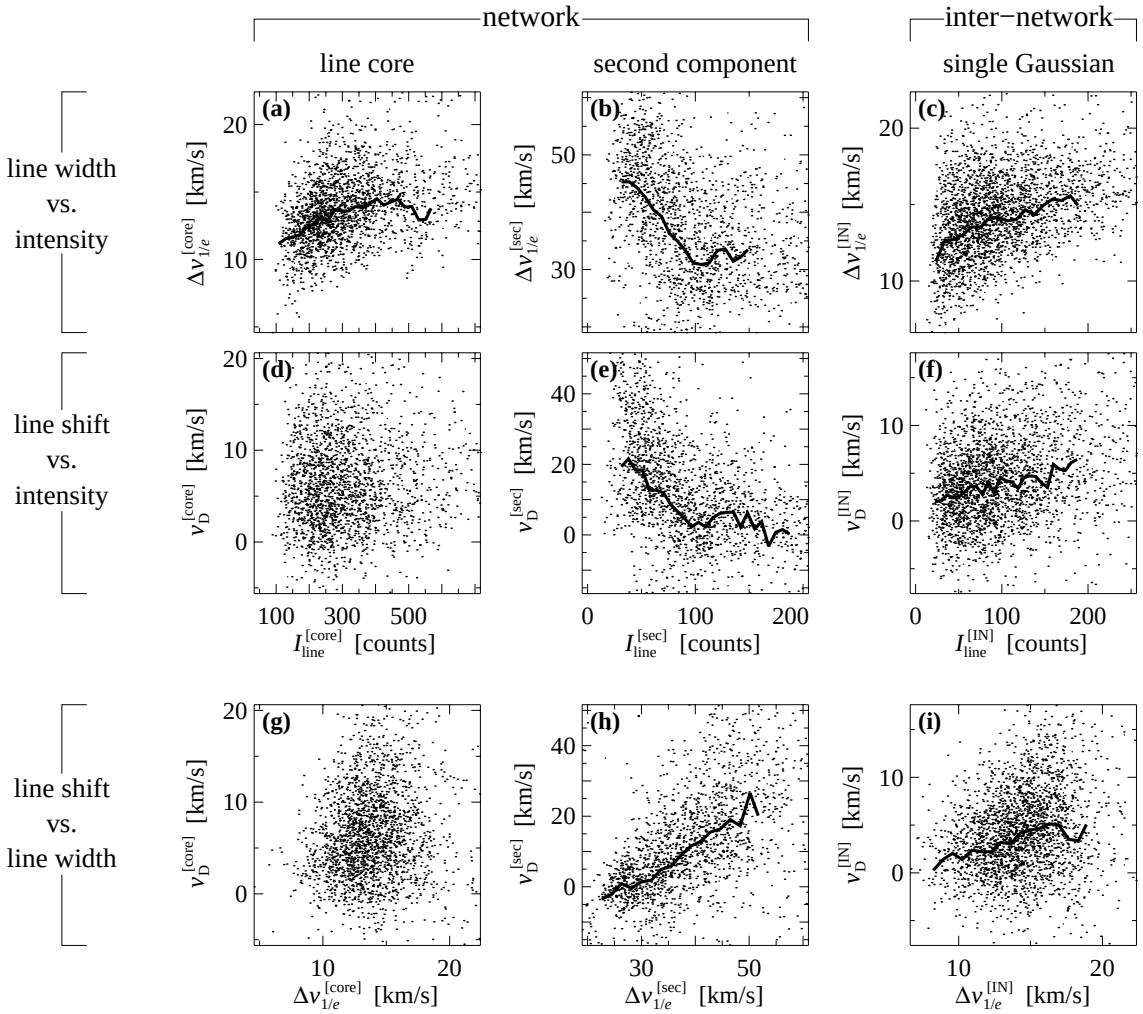

Fig. 7a–i. Correlation of the fit parameters between line intensity $I_{\rm line}$ and Doppler shift $v_{\rm D}$ as well as line width $\triangle v_{1/e}$ for the core and second components ($^{[\rm core]}$, $^{[\rm sec]}$) in the network as well as the single Gaussian profiles in the inter-network ($^{[\rm IN]}$). Positive values of $v_{\rm D}$ correspond to redshifts. The solid lines show the median variations.

line shift would be somewhat smaller for the full Sun spectrum, while the width would not be affected.

In Fig. 1 the mean spectrum is shown, i.e. integrated over a $540'' \times 300''$ rectangle. To properly fit the mean spectrum also the two Si I lines at 1547.73 Å and 1548.65 Å have to be fitted simultaneously with the two Gaussian components of the C IV profile (solid lines in Fig. 1). The fit parameters for the core and the second component are listed in Table 1. The second component contributes about 25% to the total intensity in C IV, which is slightly higher than reported in Kjeldseth Moe & Nicolas (1977).

In addition to this four Gaussian fit a fit for the two Si I lines and only a single C IV component was also performed (dotted-dashed line in Fig. 1). A simple comparison by eye and especially the drastically different $\chi^2_{\rm r}$ values as listed in Table 1 demonstrate convincingly that for C IV the double Gaussian is superior also for the mean profile. It is important to note that when considering only a single Gaussian shape the line width and also the non-thermal broadening are overestimated by about 20% (Table 1).

The line widths of the mean spectrum exceed the median values of the distribution of the individual profiles, the line shift of the second component in the mean spectrum is much smaller than the median value (cf. Table 2 and 1). For comparison the line shifts and widths of the two components of the mean spectrum are indicated by the vertical dotted lines in the histograms in Fig. 5. This effect will be discussed in Sect. 5 in terms of solar-stellar connections.

4. Transition region structure

Summarising the results described in the preceeding section (at least) three major observational classes have to be distinguished:

(1) strong network emission with narrow redshifted line profiles,
(2) weak network emission with broad profiles that are predominantly redshifted but have a significant fraction of blueshifts, and
(3) very weak inter-network emission showing little line shift.

In the following an attempt will be undertaken to interpret these classes by means of structures and physical processes in the solar atmosphere. This discussion will have a partly speculative character, especially in the broad second components. The observations presented in this study are the first of their kind that allow for a statistically meaningful analysis. More data are required to get a more complete interpretation of the new data. Investigations especially of lines formed at higher temperatures, e.g. Ne VIII (770 Å) at $6.5\,10^5$ K, will be of great value for the interpretation.

4.1. Network emission

Inspection of Fig. 3 shows the remarkable result that the spatial structures of the Doppler shifts of the narrow core and the broad second component are completely different (Sect. 3.2.2). Also the quantitative investigation of the histograms and scatter plots (Sect. 3.2 and 3.3) shows fundamental differences between the two components of the line profile. For example, the relation of line width vs. intensity is contrary for the two components (Fig. 7a, b). The conclusion is that the two components have to be formed in two (different?) physical regimes in the solar atmosphere.

Now the fundamental question becomes the identification of the source regions of the two spectral components. Here the two components will be interpreted in terms of small loops within the network (Sect. 4.1.1) and larger ones spanning across several cells (Sect. 4.1.2). In the following two subsections a motivation for this interpretation will be given. This discussion will be speculative and not unique. New data of other lines, which are planned to be analysed in the future, may provide further insight into this problem (see above).

4.1.1. Narrow components: "small" loops

Already Dowdy et al. (1986) and Porter et al. (1987) suggested that small loops might contribute a significant amount to the transition region emission and nearly all recent models for the transition region assume a loop geometry with a rather small loop length of below 5000 km. However, there are other ideas, like spicule formation (e.g. Athay 1984), that will not be discussed here.

In an attempt to understand the transition region redshifts Hansteen (1993) performed calculations of downward propagating acoustic waves caused by nanoflares in the upper part of "small" coronal loops. These semi-circular loops were about 2000 km long, corresponding to a footpoint distance of 1250 km which is at the resolution limit of SUMER. The temperature in these loops rises up to 10^6 K. In his Figs. 6 and 7 Hansteen (1993) shows the corresponding scatter plots $I_{\rm line}$ vs. $v_{\rm D}$ and $I_{\rm line}$ vs. $\triangle v_{1/e}$. These are for a single acoustic wave propagating down the loop after a nanoflare, but in general they will represent the overall picture which might simply be assumed to be the superposition of a large number of these single events.

As in the present observations, Hansteen (1993) does not find a correlation between $I_{\rm line}$ and $v_{\rm D}$ for C IV (even though a correlation might be present in O IV). In the intensity vs. width plot of the Hansteen model the width is increasing from about 12 to 15 km s^{-1} while the intensity is rising from 800 to 4000 (in arbitrary units). This matches the observed relation shown in Fig. 7a. Here the intensity is increasing from 120 to 480 counts over the same width range, which is about the same factor as in the model calculation.

This discussion shows that the emission from the line core is consistent with emission from small coronal loops anchored in the magnetic network, and it presents yet another confirmation of the Hansteen wave model of transition region Doppler shifts. Of course, other transition region models (e.g. Athay 1984; McClymont & Craig 1987; Klimchuk & Mariska 1988; Mariska 1988; Spadaro et al. 1996) might also match the shift and width vs. intensity relation, but no such scatter plots or correlations are published for them.

4.1.2. Broad components: coronal funnels?

It was suggested by Gabriel (1976) that open funnels are anchored in the network and form a canopy above the closed field structures of the inter-network. Dowdy et al. (1986) extended Gabriel's ideas by including a variety of loops with different lengths sitting below the funnels.[4]

If models for open and closed regions are compared, the transition region pressure is about a factor of 10 higher in the closed region than in the open region, if both regions are heated by the same amount (Holzer et al. 1997, their Fig. 4). As the broad second components are significantly fainter than the line cores, the broad components might be associated with coronal funnels if the narrow components are associated with closed loops as done in Sect. 4.1.1 (cf. histogtams for the intensities in Fig. 5a). Another conclusion from the lower pressure in the open region would be that the density in the open region should be lower compared to a closed region at the same temperature. In consequence the line width should be significantly higher in the funnels compared to the loops, i.e. for the second components compared to the line cores. This, again, agrees well with the observations (Fig. 5c).

For the present observations, however, the predominantely redshifted emission from the broad second components shows that the funnels cannot be magnetically open structures directly connected to the solar wind, as it is often discussed. In that case one would expect the line to be predominantly blueshifted. In addition, the closed structure of the large scale corona above the quiet Sun would contradict the assumption of the funnels being truly open.

Well above the small scale loops (Sect. 4.1.1) the funnels fill the entire volume. At transition region temperatures of 10^5 K, where C IV is formed, however, the funnels are still confined

[4] One should note that Gabriel's scenario is based on model calculations, while the picture of Dowdy et al. is a sketch motivated by observations.

to the network (see the temperature contours in Gabriel 1976; the black areas in the funnels in Fig. 8 indicate the line formation region of C IV as following Gabriel's model). This implies that when discussing emission from the coronal funnels in C IV one is still talking about emission originating from above the network – and not from above the inter-network.

The basic trends exhibited in the correlations shown in Fig. 7 for the secondary component can be understood in terms of some very simple and (hopefully) plausible assumptions:

(a) The line width, $\triangle v_{1/e}$, is a measure for the energy flux in the respective region. This holds e.g. for coronal heating by waves, but a similar positive relation between line width and energy flux density should be expected for other types of coronal heating (see Appendix B).
(b) A certain fraction of the energy flux is used to power mass motions, e.g. siphon flows in coronal loops, the up- and downward motions associated with spicules and similar phenomena, and the outflowing slow solar wind. It is reasonable to assume that the mass flux ρv is positively correlated with the energy flux. In stationary wind models this relationship is roughly linear (Hammer 1982; Hansteen & Leer 1995). Similarly, a positive relationship results also in siphon flow models of coronal loops that are heated asymmetrically (e.g. Orlando et al. 1995). And even for unsteady, stochastic heating events that temporally lift up plasma, which subsequently falls back, one expects a similar positive relationship between the energy flux and mass flux densities.
(c) The line intensity should be positively related to the density in the emitting region. It is easy to show (e.g. Hammer 1993) that in a transition region heated purely by thermal conduction, intensity and density are linearly related, while the enthalpy heating or cooling associated with down- or upflowing plasma causes small deviations from a linear relationship. The observed intensity could also be affected by variations in the filling factor of unresolved emitting threads that are lumped together within the resolution element. This would obviously cause a less than linear, but nevertheless positive, correlation, in agreement with recent observations (e.g. Griffiths et al. 1999).
(d) The last assumption, and the only one that might perhaps be not so obvious at a first glance, is that the heating energy flux density is relatively constant within the quiet sun. In fact, there is evidence that the heating flux might be proportional to the magnetic flux. This was confirmed from studies of the so-called flux-flux relations (Schrijver 1990).

By combining assumptions (a) and (b), a positive correlation between line width and and Doppler shift is obtained in agreement with Fig. 7h. The combination of assumption (d) with (c) and either (a) or (b) explains the remaining observed correlations in the middle panel of Fig. 7 for the broad second components, namely the anticorrelation between $I_{\rm line}$ and both $\triangle v_{1/e}$ and $v_{\rm D}$. This may well be an empirical confirmation that the latter assumption (d) is justified, as are the other ones.

Based on these assumptions it can be proposed that the coronal funnels are the footpoints of large coronal loops, spanning across one or more network elements. These long loops also have to have a transition region (along the magnetic field) relatively near their footpoints, where the temperature is rapidly rising to some million K. (This transition region is not observed by e.g. Yohkoh and would not be resolvable by that instrument.) The above scenario assumes that flows along the large loops are present. These flows might be caused by asymmetric heating (e.g. McClymont & Craig 1987 or Klimchuk & Mariska 1988) and have been observed in large loops (e.g. Brekke et al. 1997). In model calculations for large coronal loops Walsh et al. (1996) found the density dropping by about two orders of magnitude from the transition region at 10^5 K to coronal temperatures of several 10^6 K. Using this and assuming some expansion of the flow tube from the network into the corona one might roughly estimate an upper limit of the flow at the loop apex to be about 100 to 200 km s^{-1} by extrapolating the observed line shift in the transition region (Table 2). This would be comparable to the (adiabatic) sound speed at 10^6 K being about 150 km s^{-1}.

With this picture in mind the question arises about how to explain the dominance of redshifts for the broad second components (Fig. 5). Models for small (observationally not resolved) loops investigated syphon-type flows to explain the redshifts of the core component (e.g. McClymont & Craig 1987). At the downflowing side of the loop the material acts as a heating source in the transition region, and may furthermore even shock, both leading to a dominance of the emission on the downflow side and thus to a net redshift. If one thinks of the network being packed with feet of large loops as discussed above, one would normally have up- and downflowing legs next to each other, the downflowing ones simply dominating the emission. If it happens that a majority of upflow legs is bundled together one might also see a net blueshift in the second broad component, e.g. at solar (X,Y) $\sim (-80, 420)$ in Fig. 3.

Finally one has to ask if these large loops could be observed. EIT/SOHO and Yohkoh images of the same day the SUMER scan was performed show no indication of large loop systems in the observed region. However, this does not exclude the possibility that large magnetic loop-like structures are present. Only if their temperature rises well above 10^6 K they would be detectable by EIT and especially Yohkoh. And one has to keep in mind that if the large loops are heated e.g. only close to the footpoints, they might not reach high coronal temperatures at their apex.

4.1.3. Relation to transient events

In the preceding subsection it was discussed that the emission from the broad second components originates from large loops. It was left open though what could heat these large loops and cause the flows. In the literature it is often discussed if and how much transient events, like explosive events, nanoflares or blinkers, can contribute to the heating of the solar corona. Subsequently it will be addressed whether or not these events

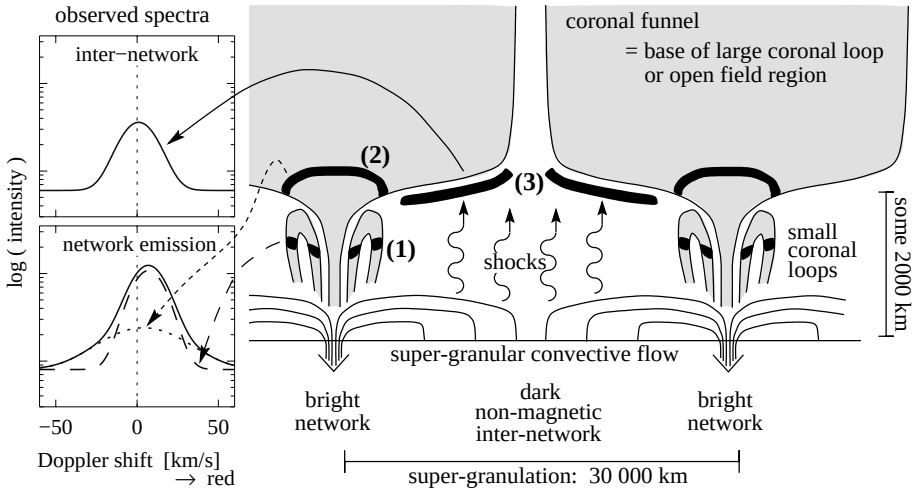

Fig. 8. Sketch of the transition region structure. The emission from the network has two components: a bright narrow one from small loops (1) and a broad second component from coronal funnels being the footpoints of large coronal loops (2). The inter-network emission originates from the interface of the shock-heated chromosphere and the above canopy (3). The black areas show the respective source regions for C IV following Gabriel (1976). The resulting spectra are shown to the left. See Sects. 4.1 – 4.3.

could directly contribute significantly to the emission in the broad second components.

One of the best know transient events are the *explosive events* (Dere et al. 1989). Because the exposure time (150 s) of the present data exceeds the typical lifetime of explosive events (40 s) as derived by Dere et al. (1989), the individual events remain unresolved. Therefore explosive events should in principle show up simply as a broadening of the emission line. Dere et al. (1989) estimated the (volumetric) emission measure in explosive events to be about $\log_{10} \mathrm{EM}_V[\mathrm{cm}^{-3}] = 41.4$ in the red and blue wing respectively, adding to a total of 41.7. This is about a factor of 4 less than found for the second components (see Table 2) and about 10% of the total emission in C IV. This compares reasonably with the finding of Linsky & Wood (1994) that the explosive events should contribute not more than 5% to the EUV emission. But the second components contribute about 25% to the total emission in C IV (Table 2 and 1), just as for the solar-like star α Cen A (Wood et al. 1997).

Recently, imaging instruments like EIT/SOHO or TRACE have been used to study flare-like events with thermal energies in the range of 10^{24}–10^{27} erg, which are often called *nanoflares*. This is based on observations of coronal plasma above 10^6 K. The explosive events as discussed above occur mainly at lower temperatures, typically below $5\,10^5$ K, and their kinetic energy content is about 10^{23} erg (Dere et al. 1989). As for the explosive events it is not definitely clear whether the nanoflares might contribute to the coronal disparate heating (cf. conflicting results of Krucker & Benz 1998 and Aschwanden 2000). However, for the discussion of the C IV line from the transition region (10^5 K) these results are hardly usable. The energy released during nanoflares at coronal temperatures (where they are observed by EIT or TRACE) has to be transported down into the transition region, most probably by heat conduction. And it is hard to estimate the amount of emission these would produce in lines like C IV.

Another class of transient events are blinkers. These are brightenings in transition region and coronal emission lasting for nearly half an hour. Harrison et al. (1999) estimated their birth rate to be about $2\,10^{-13}\,\mathrm{km}^{-2}\,\mathrm{s}^{-1}$, which is about a factor of 1000 less than the one for explosive events (Dere et al. 1989). Thus in the resolution elements of the data analysed in the present paper ($1'' \times 3''$) there is only a chance of 1 in 1000 to find a blinker! The influence of the blinkers of the formation of the second components in the network is therefore negligible.

The conclusion from this brief discussion is that it does not seem very plausible that transient events can be considered as the (direct) source of the broad second components of the C IV profile. Of course, there might be either a sufficient number of smaller events or the amount of nano- and microflares and blinkers is underestimated by the available observing techniques. It should be noted, again, that this does not mean that these events are not important for the outer solar atmosphere.

4.2. Inter-network emission

The interpretation of the weak inter-network emission can be built upon studies of the non-magnetic inter-network chromosphere performed by Carlsson & Stein (1997). They presented convincing evidence that the chromospheric emission from that region is due to acoustic shocks propagating upwards through the chromosphere. Ultimately these shocks will hit the magnetic canopy in the chromosphere that is formed by the funnels. (Unfortunately it is not yet possible to include the interaction of these shocks with the above magnetic field into the calculations.) This results in an interface between the acoustically heated non-magnetic inter-network chromosphere and the funnels having coronal temperatures and will lead to a transition region *perpendicular* to the magnetic field (Fig. 8).

At first sight one might argue that such a transition region perpendicular to the magnetic field would be extremely thin, simply because of the very low classical heat conduction perpendicular to the magnetic field. The classical heat conduction parallel to the magnetic field greatly exceeds the one perpendicular to the field by some orders of magnitude (e.g. Spitzer 1962). But it is questionable if classical heat conduction does apply at this interface. It is yet unpredictable what happens where the upward propagating shocks hit the overlying (horizontal) mag-

netic field. The interaction of the shocks with the magnetic field might well lead e.g. to turbulence and by this to an efficient heat transport across the field.

Such an interaction of the shocks with the magnetic canopy can be expected, because the plasma-β, the ratio of kinetic to magnetic energy density, is near 1 at the lower boundary of the canopy, i.e. where the shocks hit the overlying horizontal magnetic field (Solanki & Steiner 1990). Recent observations by Wikstøl et al. (2000) found observational evidence that the chromospheric shocks penetrate into the transition region, i.e. into the magnetic canopy. They found the variations in chromospheric and transition region lines (C II, O VI) formed above the non-magnetic inter-network to be correlated with continuum emission variations from the middle chromosphere formed below the canopy.

4.3. A "new view" of the transition region

It is proposed conclusively that the three observational classes as listed at the beginning of Sect. 4 correspond to the following three physical regimes on the Sun as sketched in Fig. 8.

(1) Transition region between chromospheric and coronal layers in small loops anchored with both footpoints in the same network lane (Sect. 4.1.1)
(2) Transition region of large loops with a funnel-type structure near the footpoints forming a canopy above the small loops in the network. These large loops could extend across several network cells (Sect. 4.1.2).
(3) Interface between diffuse inter-network and the canopy formed by the funnels of the large loops mentioned in (2). While the transition regions of (1) and (2) are assumed to align parallel to the magnetic field, this transition region is formed by cross-field transport (Sect. 4.2).

One has to note, though, that the physical regimes (1) and (2) do not have to correspond to different solar structures. An alternative interpretation might be that they represent the same structure in two different phases, e.g. a loop in the heating and the cooling phase. Nevertheless, based on the discussion in Sect. 4.1.1 and 4.1.2 the interpretation of it beeing two different structures seems more plausible.

4.4. Implications for coronal heating

The three different structures discussed in the preceeding section probably require different mechanisms of coronal heating. This appears to be so because the correlations of line intensity, shift and width of the narrow core and the broad second component are too different to be compatible with a single heating mechanism (Sect. 3.3).

In Sect. 4.1.1 it was discussed that the correlations for the narrow core component in the network is comparable to the ones obtained by Hansteen (1993) in his model for small loops. According to it the observations are compatible to a heating mechanism for these small loops releasing a large amount of energy in the upper part of the loops due to nanoflare-like events (Parker 1988), resulting in waves propagating downward along the loop and dissipating their energy. For other small loop models no correlations of line intensity vs. shift and width have been published. This clearly shows the need for new theoretical investigations allowing for a comparison with the presented observed correlations.

The correlations of the fit parameters of the second broad component in the network showed that it is likely that strong flows occur in the large loops (Sect. 4.1.2). These might be heated like open field regions, e.g. due to (high-frequency) Alfvén waves as suggested by e.g. Tu & Marsch (1997), Cranmer (1998) or Hollweg (1999). However, further work has to be done to check if these open field models do really apply to the large loops and how this does compare to non-flow large loop models like the one of Priest et al. (1998) that would not produce the observed systematic line shifts of the broad components.

Following the discussion in Sect. 4.2 the transition region emission from the inter-network is originating from a region heated in a completely different manner. This source region would not be heated in a usual way, but the transition region temperatures would be maintained by heat conduction perpendicular to the field, induced probably by turbulence due to the interaction of the upward-propagating shocks of the non-magnetic inter-network with the hotter horizontal magnetic structures above.

This discussion can not provide definite answers to the heating problem, it just gives some hints on future work, both theoretical and observational. But it shows that there are different heating mechanism acting in the solar atmosphere, depending on which structures are considered.

With the present observations alone it is not finally decidable whether the source regions of the narrow and broad component in the network are heated by the same amount. Too many unknowns, especially the filling factor, are playing a crucial role. One could perform a very rough estimate though showing that the energy fluxes do not contradict the assumption of uniform heating, at least for the Alfvén wave case.

From the observed non-thermal line width one can estimate the energy flux into the corona through the observed region (Appendix B). It is then possible to compare the energy fluxes in the source regions of the narrow core and the second broad component by taking their quotient, $Q \approx F^{[\mathrm{core}]}/F^{[\mathrm{sec}]}$. The non-thermal widths, ξ, are listed in Table 2, the emission in a conductively heated transition region is essentially proportional to the density, $I_{\mathrm{line}} \propto \rho$ (e.g. Hammer 1993).

Now the quotients for a sound wave, an Alfvén wave and a turbulent cascade are given by $Q_{\mathrm{sound}} \approx 0.5$, $Q_{\mathrm{Alfvén}} \approx 0.1\,(B_{\mathrm{core}}/B_{\mathrm{sec}})$ and $Q_{\mathrm{turb}} \approx 0.03$. B_{core} and B_{sec} are the magnetic field strength at the source regions of the two components. While for the turbulent cascade heating a quite large ratio of the filling factors of about 50 would be needed to have uniform heating, this is only a factor of two for propagation of sound waves. For the Alfvén wave propagation one needs some estimate of the magnetic field. As discussed above the density in an open region is about a factor of 10 less than in a closed re-

gion of the same temperature (Holzer et al. 1997), which might also apply for the coronal funnels. Thus the funnels can be expected to be more stretched out vertically than the surrounding closed field regions, i.e. C IV is formed in the funnels at higher altitudes than in closed regions. Above the smaller loops one must expect some sort of canopy effect for the funnels, which in turn have a significant lower magnetic field strength at the same temperature level. In conclusion it seems not unrealistic to have the same energy flux due to Alfvén waves in the funnels and the closed regions, i.e. $Q_{\rm Alfvén} \approx 1$.

As noted in Sect. 3.4 the non-thermal broadening, ξ, would be over-estimated by about 20%, if only a single Gaussian fit would be applied. Thus, when deriving heating rates by means of wave-transported energy flux into the corona, one has to apply a double Gaussian fit to the transition region spectra. Otherwise, because the energy flux is proportional to ξ^n with $n > 2$ (see Appendix B), the heating rate would be over-estimated by at least 40%.

5. Solar–stellar connections

The discussion of the multi-component structure of the solar transition region showed that one has to deal with at least three different types of transition region emission. On the Sun the network emission from the coronal funnels and the small loops can not be spatially separated in principle, because the former originates in a region closely above where the latter one is formed (see Fig. 8). Only the inter-network emission can be spatially resolved for the solar case.

When observing a star this problem of mixing emission from different physical regimes from different locations is even worse, of course. Nevertheless, Wood et al. (1997) showed that for a large number of stars with different activity level a two component structure of the transition region line profiles is found, similar to that of the Sun. They got a simple correlation of the relative width of the second broad components with stellar activity.

But one has to be very carful when interpreting the stellar spectra in a quantitative way. This might be illustrated by comparing the parameters for the profiles of the individual spatially resolved spectra (Fig. 5, Table 2) and the mean spectrum (Fig. 1, Table 1). As the mean spectrum shown here represents a quiet-Sun-as-a-star spectrum (see Sect. 3.4) the effects discussed in the following might as well apply to the spectra of solar-like stars (e.g. α Cen A, a G2 V star like the Sun).

5.1. Implications for line width analysis

The line widths, $\triangle v_{1/e}$, of the mean spectrum in both the narrow core and the broad second component exceed the median values of all the individual spectra (Fig. 5c). This is because for the mean spectrum of the whole field of view the Doppler shifts of the individual spectra are not resolved but smeared out. Assume for the moment that all individual spectra would have the same intensity and the same width, $w_{\rm i}$, and that their Doppler shift distribution is Gaussian. If then the width of the histogram of the shifts has the width $w_{\rm h}$, the mean line profile would have the line width $(w_{\rm i}^2 + w_{\rm h}^2)^{1/2}$.

When approximating the histograms for the line shift in Fig. 5b by Gaussians, the exponential widths of the distributions are about 8 km s^{-1} and 11 km s^{-1} for the core and second component. Adding these widths of the line shift histograms to the median values of the line width distributions (13 km s^{-1} and 33 km s^{-1}), this results in corrected "mean" values of 15 km s^{-1} and 35 km s^{-1}. This agrees well with the widths of the mean spectrum (cf. $\triangle v_{1/e}$ in Table 1).

The conclusion is that the line width of a stellar spectrum over-estimates the mean value of the line widths of the emission from the actual structures on the stellar surface. This thought is not new, of course, but with the present observations the difference can be quantified to be about 15% and 5% for the narrow core and the broad second component respectively. This is even more pronounced when comparing the non-thermal broadenings, ξ, where the effect is more than 50% for the line core. Also the center-to-limb variation of the line shift would lead to an additional broadening of the width of the Sun-as-a-star spectrum by a couple of km s^{-1} (see Sect. 3.4).

This result is important when estimating the (mechanical) energy flux into a stellar corona from line width observation (see Appendix B). If the line widths are not corrected for the effects mentioned above, the heating might be seriously over-estimated (Sect. 5.3).

5.2. Implications for line shift analysis

The Doppler shift of the core component of the mean spectrum (6.2 km s^{-1} to the red) is comparable to the median value of the distribution of all individual core component shifts. This is not true for the second components. The median value for the second component Doppler shifts is 5.3 km s^{-1} to the red, but the second component of the mean spectrum is nearly unshifted (0.5 km s^{-1} red).

This is resolved by studying the intensity vs. Doppler shift relations (Fig. 7d and e). While there is no correlation for the line core, the redshift of the broad second component is dropping dramatically from 20 km s^{-1} to zero with increasing intensity (maybe even changing to blueshifts for highest intensities). Taking the mean spectrum implies a weighting with intensity: small red and blueshifts are favoured over more frequent and stronger redshifts. This results in an only small shift of the broad component in the mean spectrum. For the line core there is no correlation, i.e. no weighting, and the median shift of the individual profiles and the shift of the mean profile are close.

For α Cen A Wood et al. (1997) find a blueshift of the broad second component of 2 km s^{-1}. At first sight one might interpret this in a simple-minded way as a globally present outflow, i.e. a stellar wind, already deep in the transition region of the star. However, one might safely assume that the network structure of the solar-like star α Cen A is not too different from the Sun. Then following the above discussion this small blueshift is more likely also caused by a weighting effect, but generally the second component is redshifted.

This discussion shows that one has to be quite careful when interpreting (by definition mean) stellar spectra, because they may be "contaminated" by a minor fraction of an area with high intensity that is *not typical* for the star.

5.3. Interpretation of stellar observations

Studying a sample of stars enables one to study the parameters of the emission line profiles as a function of stellar parameters, like surface gravity or transition region pressure. This opens a parameter space not available to a solar physicist. Due to this Wood et al. (1997) concluded that the source regions of the narrow components might be heated by energy dissipation in a turbulent cascade. This is based on the variation of the line width with electron pressure in the line formation region and the surface gravity.

This type of stellar study is also and especially very important to understand the heating of the solar corona. But nevertheless one should be aware of some of their shortcomings. Hopefully this work contributes to avoid those traps.

The two main problems in interpreting stellar observations are that (1) the emission might be dominated by intense emission from small regions and (2) a multitude of different structures exist. On top of that these different structures are probably heated in different ways (see Sect. 4.4). Thus it will be hard to draw a final conclusion on *the* heating mechanism present on a star, because there is no such thing. And it might even be problematic to find the dominant one. The relation of line width to electron pressure for a number of stars as used by Wood et al. (1997) might indeed be due to the fact that the transition region is heated by a turbulent cascade as they conclude. But one could also come up with a situation where different distributions of structures on different stars might mimic the same relation. This is especially true when one considers a wide range of activity levels in a multi-star study.

One way to deal with these problems is to learn from the Sun and put together a kind of "empirical forward model" which could work at least for solar-type stars. One could use standard models for the emission from the different structures as mentioned in Sect. 4.3 and calculate the total emission from these structures following e.g. the distributions as presented in this paper. By varying the parameters for the different models one could come up with one or several possible scenarios. When comparing the scenarios of different stars one might end up with a conclusive picture at some point. This procedure is probably not going to point out one solution only. But should one really expect a simple unique answer for the multitude of stars?

6. Conclusions

A quiet Sun analysis of the C IV (1548 Å) line was presented distinguishing between three different observational classes: Emission in a narrow line core and in a broad second component originating from the bright network as well as emission in single Gaussian profiles from the inter-network. This study allowed for the first time a statistically meaningful investigation of the broad second Gaussian components of the line profile.

The broad second components, which are restricted to the bright network, are blueshifted compared to the narrow line core, but are still predominantly redshifted. However, in contrast to the line core, quite large areas show also blueshifts in the broad second components (Sect. 3.1 and 3.2.2).

Over all the broad second component contributes about 25% to the total C IV intensity (Sect. 3.4). The transition region inter-network emission is even weaker than the one from the broad components in the network (Sect. 3.2.1). The correlations of line intensity, shift and width show that the emission from the three observational classes originate from different physical regimes (Sect. 3.3 and 4). Previously reported correlations of line intensity vs. shift of the line core are only a signature of the cell-network-structure (e.g. Peter 1999) and are not seen within the bright network elements (Sect. 3.3). To consider the broad second components is also of importance for the estimation of the energy input into the corona. If only a single Gaussian profile is assumed, the mechanical energy flux into the corona by means of waves would be over-estimated significantly by 40% (Sect. 4.4).

A first interpretation of these new observational results was presented. The narrow line core could be formed in small loops (lengths below $\sim$5000 km) anchored with both footpoints in the network, which are probably heated by nanoflare-induced waves as suggested by Hansteen (1993) (Sect. 4.1.1). The broad second component could be formed in the funnel-type footpoint regions of large coronal loops spanning across one or several network elements. The footpoint regions of these loops might be identified with the coronal funnels as proposed by Gabriel (1976). The line shifts indicate that strong flows are present in these large loops (Sect. 4.1.2). The observations are compatible with the assumption that both, the large and the small loops, are heated by the same amount of energy flux, even though the heating mechanisms in these structures are different (Sect. 4.4). The transition region inter-network emission could originate from an interface between the non-magnetic chromosphere and an overlying canopy formed by the funnels of the large loops. Here the upward propagating shocks from the chromosphere might interact with the above horizontal magnetic field allowing an efficient transport of heat also across the field (Sect. 4.2).

This would put together a new picture of the structure of the quiet Sun transition region with at least three different physical regimes (Sect. 4.3). These structures differ not only in size or temperature, but are of a different quality. However, more work especially on lines originating from other temperatures than the middle transition region, e.g. S VI (933 Å) and Ne VIII (770 Å) formed at 1.9 and $6.5\,10^5$ K, has to be done before final conclusions can be drawn.

The fact that the transition region is made of qualitatively different physical structures sheds also new light on the interpretation of stellar transition region data. It was shown that it could be misleading to simply interpret the mean spectrum of the stellar disk assuming implicitly that the observed emission

comes from either a single structure or a limited number of evenly distributed structures. Especially when comparing stars of different activity levels one has to be careful, because one does not know how the distribution of structures will change with activity. The solar data presented here may be used for a new interpretation of spectra of quiet solar-like stars as one might use the distribution of structures found for the Sun for these stars as well (Sect. 5).

This investigation may have raised more questions than answers. But it has also shown the feasibility of analysing weak broad components of solar transition region spectra and its power in studying the heating processes of the corona.

Acknowledgements. With great pleasure I would like to thank Reiner Hammer for the numerous interesting and animating discussions and him and Phil Judge for carefully reading the manuscript. I acknowledge the open data policy of the SUMER team and Klaus Wilhelm (PI). Thanks are also due to Don Hassler who initiated the sequence for the observations presented in this paper. The SUMER project is financially supported by DLR, CNES, NASA and the ESA PRODEX programme (Swiss contribution).

Appendix A: emission measure

To be able to compare the present results on the emissivity of the narrow line core and the broad second components with the literature, the emission measure is calculated as well. Following Mariska (1980) and Pottasch (1964) the power emitted from a volume V below the surface $\mathcal{A}$ is given by

$$P\ [\mathrm{erg\,s^{-1}}] \ = \ 2.2\,10^{-15}\,A_{\rm el}\,g_{\rm eff}\,f\,{<}G(T){>}\int_V n_{\rm e}^2\,\mathrm{d}V.$$

For C IV (1548 Å) the abundance $\log_{10} A_{\rm el} = -3.44$ is taken from Anders & Grevesse (1989), the effective Gaunt factor $g_{\rm eff} = 0.32$ and the oscillator strength $f = 0.19$ are calculated from Landini & Monsignori Fossi (1990) and the contribution function $<G(T)> = 3\,10^{-4}$ is calculated following Mariska (1992) using the ionisation equilibrium from Arnaud & Rothenflug (1985).

The (average) solar surface flux is given by the power per emitting surface, $F_\odot{=}P/\mathcal{A}$. This finally defines the volumetric emission measure

$$\mathrm{EM}_V\ [\mathrm{cm^{-3}}] = \int_V n_{\rm e}^2\,\mathrm{d}V = \frac{\mathcal{A}\,[\mathrm{cm^2}]\ F_\odot\ [\mathrm{erg\,cm^{-2}\,s^{-1}}]}{2.2\,10^{-15}\,A_{\rm el}\,g_{\rm eff}\,f\,{<}G(T){>}}.$$

(See also the textbook of Mariska 1992. Most authors give the emission measure EM_V for the whole star, i.e. the volume V is a complete shell and the area is the surface of the star or the Sun, $\mathcal{A}{=}4\pi R_\odot^2$. Often then the observed radiant flux F at the distance R is used instead of the solar surface flux, i.e. $F/F_\odot{=}R_\odot^2/R^2$.)

In the case of Mariska (1980) the emitting surface $\mathcal{A}$ was the whole field of view ($2''{\times}60''$ with the NRL spectrograph on Skylab, SO82B). In the present case $\mathcal{A}$ is the size of the spatially resolved structures, i.e. $1''{\times}3''$ as outlined in Sect. 2.1 ($\mathcal{A}{\sim}1.5\,10^{16}\,\mathrm{cm^2}$).

Often the volumetric emission measure is rewritten as an integral over height, $\mathrm{EM}_h = \int n_{\rm e}^2\,\mathrm{d}h$, where the volume element $\mathrm{d}V$ is substituted by the area $\mathcal{A}$ and the height $\mathrm{d}h$, $\mathrm{d}V = \mathcal{A}\,\mathrm{d}h$. Usually then the radiance $I_{\rm line}$ is used instead of the solar surface flux $F_\odot{=}\pi I_{\rm line}$ (see above) and EM_h is independent of $\mathcal{A}$.

With the above numbers the emission measures at $\sim 10^5$ K are given for C IV (1548 Å) simply by

$$\begin{aligned}\mathrm{EM}_V\ [\mathrm{cm^{-3}}] \ &= \ 1.1\,10^{42}\ F_{\odot,\,\mathrm{C\,IV}}\ [\mathrm{W\,m^{-2}}],\\ \mathrm{EM}_h\ [\mathrm{cm^{-5}}] \ &= \ 2.1\,10^{26}\ I_{\mathrm{line,\,C\,IV}}\ [\mathrm{W\,m^{-2}\,sr^{-1}}].\end{aligned}$$

The resulting emission measures of the respective median values are listed in Table 2. The mean values for the quiet Sun, i.e. the weighted average over network and inter-network, agree well with the values listed e.g. by Raymond & Doyle (1981) and Mariska (1980). The differences are basically due to of different values of $A_{\rm el}$, $g_{\rm eff}$, f and $<G(T)>$. Please note that the values of Mariska (1980) are for the limb, which are about a factor of 10 higher than on the disk because of the center-to-limb brightening (Wilhelm et al 1998).

Appendix B: spectral signatures of heating

All the transition region emission lines have line widths in excess of their thermal width, quantified by the non-thermal broadening, ξ. This is defined through the line width $\triangle v_{1/e}^2 = 2v_{\rm ion}^2 + \xi^2$, where $v_{\rm ion} = (k_{\rm B}T/m_{\rm ion})^{1/2}$ is the isothermal ion sound speed.

The non-thermal broadening can be interpreted in terms of a signature of the heating mechanism. This broadening might be due e.g. to waves propagating through the observed region or due to turbulent motions associated with magnetic reconnection (Heyvaerts & Priest 1993), both ultimately leading to plasma heating. Assuming the energy is transported into the corona by waves the energy flux into the corona is given by $F = \rho\,v_{\rm rms}^2 v_{\rm prop}$, with the density ρ (see e.g. Brown & Jordan 1981).

For a sound wave the propagation speed, $v_{\rm prop}$, would be the sound speed, i.e. about $48\,\mathrm{km\,s^{-1}}$ at the source region of C IV. Because the root-mean-square velocity is given by $v_{\rm rms}^2 = 3/2\,\xi^2$, the non-thermal broadening, ξ, is related to the energy flux into the corona, i.e. the strength of the heating. Thus for a sound wave the energy flux is proportional to the square of the non-thermal broadening, $F_{\rm sound} \propto \rho\,\xi^2$. Similarly for an Alfvén wave the energy flux is also proportional to the magnetic field B, $F_{\rm Alfvén} \propto \sqrt{\rho}\,\xi^2 B$, because the wave propagates with the Alfvén speed, $v_{\rm A}{\propto}B/\sqrt{\rho}$. If a turbulent cascade is considered, the energy flux is related to the non-thermal broadening by $F_{\rm turb} \propto \rho\,\xi^3$ (e.g. Wood et al. 1997).

In this sense the non-thermal broadening is a signature of the *cause*, i.e. the heating process or the transport of the energy itself. In contrast, the observed intensity and the Doppler shift provide information on the *effect* of the heating process. For example, one would naively expect that the larger the energy flux into the corona, the higher the observed intensity. But it does not have to be as simple as that, as the energy could also be used to lift material out of the gravity well or might be converted into an enthalpy flux, i.e. in a plasma flow (like in the solar wind or for syphon flows).

The Doppler shift can also be considered as a signature of the effect of the heating process. The well known red- and blueshifts in solar transition region lines are not completely understood yet, even though some progress was made recently on the observational (Peter & Judge 1999) as well as on the modelling side (Teriaca et al. 2000 based on Hansteen 1993). However, one has to note that these studies concentrated only on the core components of the transition region lines and that as yet no modelling efforts have been undertaken to understand the broad second components.

References

Anders E., Grevesse N., 1989, Geochim. Cosmochim. Acta 53, 197
Arnaud M., Rothenflug R., 1985, A&AS 60, 425
Aschwanden M.J., 2000, Sol. Phys., in press
Athay R.G., 1984, ApJ 287, 412
Bevington P.R., Robinson D.K., 1992, Data Reduction and Error Analysis for the Physical Sciences. McGraw-Hill, New York
Brekke P., Kjeldseth Moe O., Harrison R.A., 1997, Sol. Phys. 175, 511
Brown A., Jordan C., 1981, MNRAS 196, 757
Carlsson M., Stein R.F., 1997, ApJ 481, 500
Charbonneau P., 1995, ApJS 101, 309
Cranmer S.R., 1998, ApJ 508, 925
Dammasch I.E., Hassler D., Curdt W., Wilhelm K., 1999, Space Sci. Rev. 87, 161
Dere K.P., Mason H.E., 1993, Sol. Phys. 144, 217
Dere K.P., Bartoe J.-D.F., Brueckner G.E., 1984, ApJ 281, 870
Dere K.P., Bartoe J.-D.F., Brueckner G.E., 1989, Sol. Phys. 123, 41
Dowdy J.F., Rabin D., Moore R.L., 1986, Sol. Phys. 105, 35
Gabriel A.H., 1976, Phil. Trans. R. Soc. Lond. A 281, 339
Gallagher P.T., Phillips K.J.H., Harra-Murnion L.K., Keenan F.P., 1998, A&A 335, 733
Griffiths N.W., Fisher G.H., Woods D.T., Siegmund O.H.W., 1999, ApJ 512, 992
Hammer R., 1982, ApJ 259, 779
Hammer R., 1993, In: Linsky J.L., Serio S. (eds.) Physics of solar and stellar coronae. Kluwer, p. 591
Hansteen V.H., 1993, ApJ 402, 741
Hansteen V.H., Leer E., 1995, J. Geophys. Res. 100, 21577
Harrison R.A., Lang J., Brooks D.H., Innes D.E., 1999, A&A 351, 1115
Hassler D.M., Dammasch I.E., Lemaire P., et al., 1999, Sci 283, 810
Heyvaerts J., Priest E.R., 1993, ApJ 390, 297
Hollweg J.V., 1999, J. Geophys. Res. 104, 505
Holzer T.E., Hansteen V.H., Leer E., 1997, In: Jokipii J.R., Sonett C.P., Giampapa M.S. (eds.) Cosmic winds and the heliosphere. Univ. of Ariziona Press, Tucson, p. 239
Kjeldseth Moe O., Nicolas K.R., 1977, ApJ 211, 579
Klimchuk J.A., Mariska J.T., 1988, ApJ 328, 334
Krucker S., Benz A.O., 1998, ApJ 501, L213
Landini M., Monsignori Fossi B.C., 1990, A&AS 82, 229
Linsky J.L., Wood B.E., 1994, ApJ 430, 342
Mariska J.T., 1980, ApJ 235, 268
Mariska J.T., 1988, ApJ 334, 489
Mariska J.T., 1992, The solar tansition region. Cambridge University Press
McClymont A.N., Craig I.J.D., 1987, ApJ 312, 402
Orlando S., Peres G., Serio S., 1995, A&A 294, 861
Parker E.N., 1988, ApJ 330, 474
Peter H., 1999, ApJ 516, 490
Peter H., Judge P.G., 1999, ApJ 522, 1148
Porter J.G., Moore R.L., Reichmann E.J., et al., 1987, ApJ 323, 380
Pottasch S.R., 1964, Space Sci. Rev. 3, 816
Priest E.R., et al., 1998, Nat 393, 545
Raymond J.C., Doyle J.G., 1981, ApJ 245, 1141
Schrijver C.J., 1990, A&A 234, 315
Solanki S.K., Steiner O., 1990, A&A 234, 519
Spadaro D., Lanza A.F., Antiochos S.K., 1996, ApJ 462, 1011
Spitzer L., 1962, Physics of fully ionized gases. Interscience, New York
Teriaca L., Doyle J.G., Erdélyi R., Sarro L.M., 2000, A&A, in press
Tu C.-Y., Marsch E., 1997, Sol. Phys. 171, 363
Walsh R.W., Bell G.E., Hood A.W., 1996, Sol. Phys. 169, 33
Wikstøl Ø., Hansteen V.H., Carlsson M., Judge P.G., 2000, ApJ 531, 1150
Wilhelm K., Curdt W., Marsch E., et al., 1995, Sol. Phys. 162, 189
Wilhelm K., Lemaire P., Dammasch I.E., et al., 1998, A&A 334, 685
Wood B.E., Linsky J.L., Ayres T.R., 1997, ApJ 478, 745